Mechanics of Planar Periodic Microstructures

by

Sharon M. Prange

SUBMITTED TO THE DEPARTMENT OF MECHANICAL ENGINEERING IN PARTIAL FULFILLMENT OF THE REQUIREMENTS FOR THE DEGREE OF

BACHELOR OF SCIENCE
AT THE
MASSACHUSETTS INSTITUTE OF TECHNOLOGY

JUNE 2007

Signature of Author:_____
Department of Mechanical Engineering
May 11, 2007

Certified by:_____
Mary C. Boyce
Gail E. Kendall (1978) Professor of Mechanical Engineering
Thesis Supervisor

Accepted by:_____
John H. Lienhard V
Professor of Mechanical Engineering
Chairman, Undergraduate Thesis Committee

Mechanics of Planar Periodic Microstructures

by

Sharon M. Prange

Submitted to the Department of Mechanical Engineering
on May 11, 2007 in partial fulfillment of the
requirements for the Degree of Bachelor of Science in
Mechanical Engineering

ABSTRACT

The deformation of two-dimensional periodically patterned elastomeric sheets has been shown to trigger interesting pattern changes that are both repeatable and predictable (Bertoldi et al., 2007). Here, both square and hexagonal lattices of these sheets under axial compression are investigated both with empty voids, and also with inclusions introduced into the voids in specified patterns. A local buckling instability in the square lattice and shear instability in the hexagonal lattice trigger the change in pattern in the structure upon reaching a critical stress during compression. Experimental and numerical results are obtained that show the ability to predict and control the pattern changes that are triggered. The shape of the pattern change, the areas of the lattice in which it is triggered, and the extent to which the pattern is accentuated can all be controlled in a predictable manner. While the results here are on the millimeter length scale, they should also be applicable at the micro- and nano-scales, leading to photonic and phononic applications.

Thesis Supervisor: Mary C. Boyce
Title: Gail E. Kendall (1978) Professor of Mechanical Engineering

1. Introduction

Cellular solids are materials composed of a system of beams or plates that connect to form the edges or faces of cells. They can exist in either two or three dimensions (Gibson and Ashby, 1997). Cellular solids are found widely in nature, as well as synthetically manufactured in a variety of forms. They have a wide range of applications in mechanical, acoustic, and thermal disciplines. The deformation of these materials can lead to varying micro-structure instabilities that are usually localized (Gibson and Ashby, 1997) or which may produce pattern changes that are predictable and repeatable (Mullin et al., 2007; Bertoldi et al., 2007).

In particular, the deformation of two-dimensional periodically patterned elastomeric sheets has shown the triggering of interesting pattern changes that can be predicted through numerical simulation (Bertoldi et al., 2007). Both square and hexagonal lattices of circular voids cut into an elastomeric sheet have been investigated. The results show that a pattern transformation is triggered as the result of a local elastic instability. With the deformation occurring in the elastic regime, the pattern change is both reversible and repeatable. The square and hexagonal lattices have different modes of failure which lead to distinct pattern changes. Different spacing between holes in the lattice leads to varying critical loads at which the pattern change starts. The shape of the pattern change and the load at which it occurs can therefore be controlled to some extent. The structure can be designed to function specifically for particular applications.

With the square lattice a local buckling instability leads to the pattern transformation. The ligaments between the voids can be conceptually modeled as columns which buckle at a critical load when under compressive stress. At lower stresses the voids are uniformly compressed, and then as buckling of the ligaments occurs the voids take on elliptical shape. The ellipses are aligned in alternating directions so that every other void has its major axis vertical.

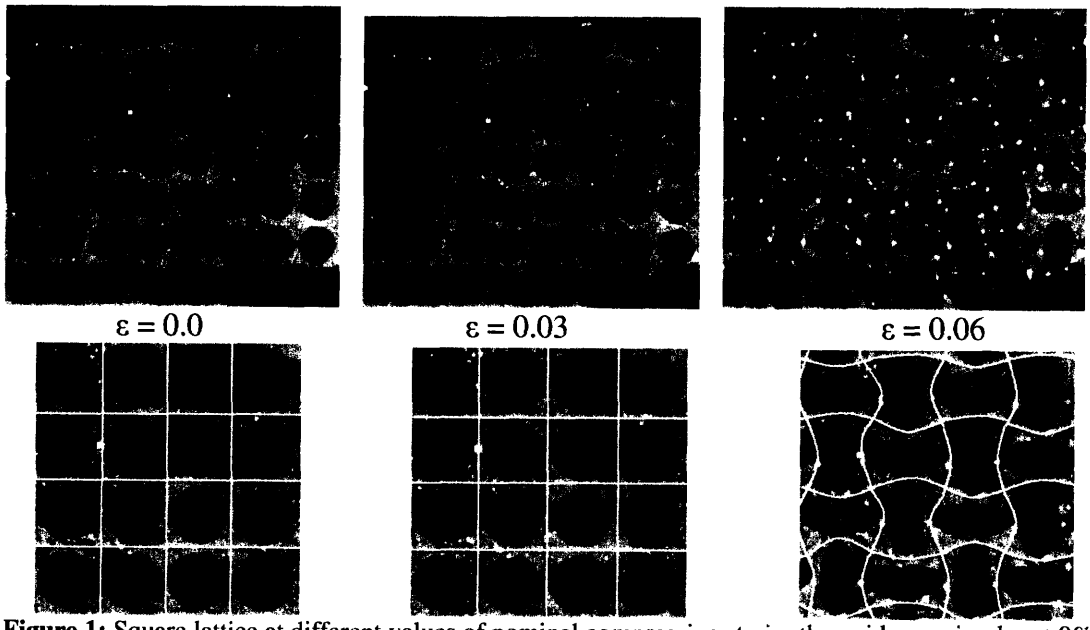

Figure 1: Square lattice at different values of nominal compressive strain: the voids are circular at 0% strain, the voids are uniformly compressed at 3% strain, then the pattern change is seen at 6% strain. Bottom images show lines of the lattice; buckling is seen at 6% strain.

The hexagonal lattice has a local shear instability that triggers the pattern transformation. The voids are uniformly compressed at lower stresses, then form alternating rows of sheared voids upon reaching a critical stress level.

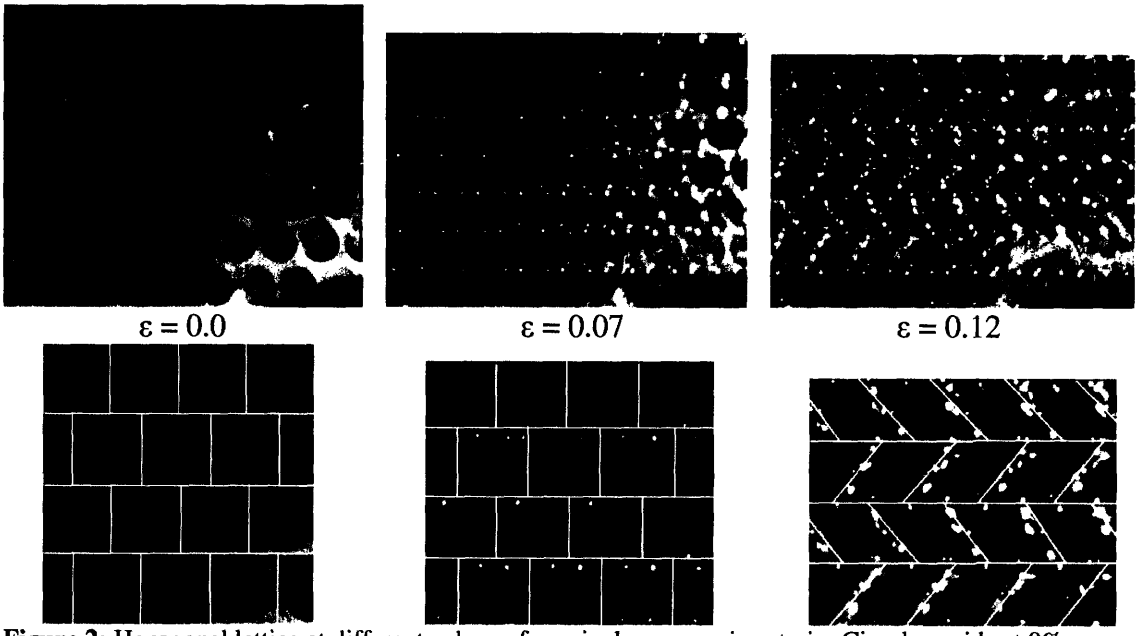

Figure 2: Hexagonal lattice at different values of nominal compressive strain: Circular voids at 0%, uniform compression at 7%, shear voids in alternating rows at 12%. Bottom images show lines of the lattice; shear is seen at 12% strain.

The shape of the pattern change can also be investigated using finite element analysis. A buckling analysis of the lattice provides different modes of buckling and the estimated load at which buckling occurs. The experimental results show only the first mode of buckling because it requires the lowest load to initiate buckling. However, the higher modes may be produced by suppressing the first mode. By introducing inclusions with a lower shear modulus than the lattice material, the first mode of the overall structure can be suppressed in favor of a particular higher mode. The placement of the inclusions can dictate which mode will be favored.

The placement of inclusions into the voids of a patterned elastomeric sheet in order to preferentially trigger different modes of buckling is investigated in this paper. The problem is approached through both experimental tests and finite element modeling. Both square and hexagonal lattices cut into an elastomeric sheet of material will be used, and the behavior under axial compression examined. The inclusions will be placed in different patterns in order to preferentially trigger different buckling modes of the system. The stress-strain behavior, as well as the overall pattern of deformation will both be studied. Numerical results will be found using finite element analysis, and the accuracy with which the model can predict the actual experimental results will be determined.

2. Theory and Modeling

2.1 Conceptual Model

In order to conceptually understand the instability that leads to the pattern transformation, the vertical ligaments are treated as columns subjected to compressive loading. The deformation of a vertical column subjected to a compressive load will exhibit two regimes of behavior. With smaller loads, the column will exhibit linear elastic compression force versus displacement behavior. With a uniaxial load, a linear relationship of

$$\sigma = E\varepsilon \tag{1a}$$

$$P = \frac{AE}{L}\delta \tag{1b}$$

where σ is the stress in the column, ε is the axial strain, and E is the Young's modulus; P is the axial force, A is the cross-sectional area, L is the length, and δ is the change in length. This behavior holds until the load reaches a critical value. As the load is increased, the stability of the beam changes. At some critical point, it requires less energy for the beam to bend than to uniformly compress. At this critical point the beam is at a border between stability and instability, or in neutral equilibrium. When the load becomes greater than the critical load, the beam is unstable, and will change from its original configuration by bending- this is the buckling phenomenon.

The uniform compression analysis assumed a perfect beam with no imperfections, and a perfectly centered force. Instead, small imperfections lead to less than perfect loading conditions. We can consider an imperfection in the form of the load being applied a small distance e from the center, creating a small moment which can bend the beam:

$$M = Pe \tag{2}$$

This will result in some lateral displacement y of the beam. For small loads this displacement is small, but as the load increases the displacement becomes large enough for bending to be more favorable than compression. The load at which the displacement becomes large is the critical load P_{cr}, and occurs at different values depending on the geometry of the beam and its boundary conditions. At loads below P_{cr}, the beam is stable and deforms by uniform compression, whereas at loads above P_{cr} the beam is unstable and buckles, then deforms by bending. When this unstable point is reached, the beam will buckle, and will no longer follow a linear elastic force-deformation behavior; the beam may still be elastic, but the force-deformation behavior will now be non-linear.

A buckling analysis can be done for a simple rectangular beam with pinned-pinned end boundary conditions. The ligaments in the lattice structures can be approximated by this model.

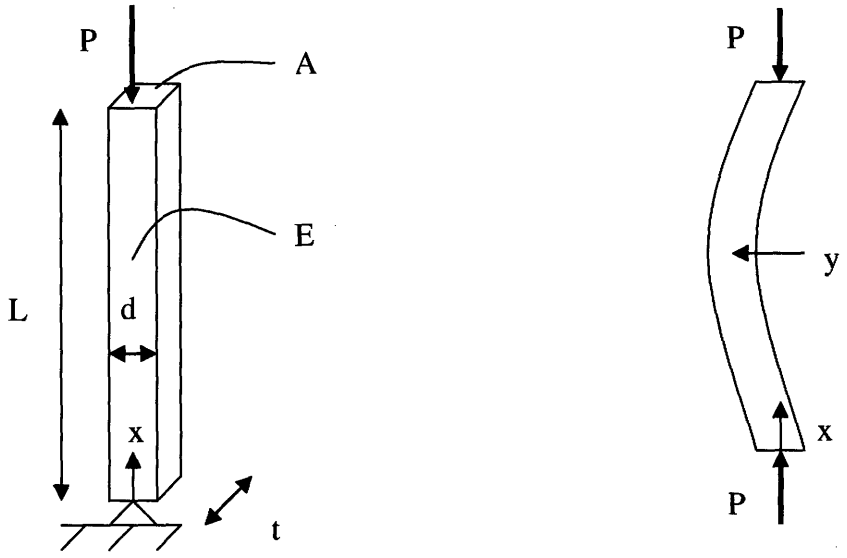

Figure 3: 1) Beam with pinned-pinned ends, length L, width d, thickness t, Young's Modulus E, and cross-sectional area A. 2) Buckled beam, with lateral displacement y.

In order to find P_{cr} for a given beam, the point at which the restoring forces on the beam just balance the upsetting forces must be found. This is the point where the beam is in neutral equilibrium, and an increased load will cause the beam to become unstable and buckle. The deflection of a beam can be shown to be

$$\frac{d^2y}{dx^2} = \frac{M}{EI} \tag{3}$$

where E is the Young's modulus and I is the moment of inertia. By substituting in equation (2), the relationship

$$\frac{d^2y}{dx^2} + \frac{P}{EI}y = 0 \tag{4}$$

is found. With the boundary conditions for a pinned-pinned column of length L of $y = 0$ at $x = 0$, and $y = 0$ at $x = L$, the solution to this differential equation is

$$(\frac{P}{EI} - \lambda^2)C\sin(\lambda x) = 0 \tag{5}$$

where C is the integration constant, and $\lambda = \frac{n\pi}{L}$. By setting the term in parentheses equal to zero the critical load at which buckling occurs in a column with pinned-pinned boundary conditions can be found

$$P_{cr} = EI\left(\frac{n\pi}{L}\right)^2 \tag{6}$$

This expression shows that a longer beam results in a much lower load required to initiate buckling.

The behavior of the latticed material can be modeled as the buckling of beams. The ligaments between the voids can be modeled as columns with a uniaxial compression load applied to them. While the actual shape of the material between voids is not rectangular, they can be approximated to follow the same buckling behavior. The length

L of the column can be seen as a function of the radius R of the voids and the ligament length l in the lattice. The width d is a function of the width of the ligament and the curvature of the void, and t represents the thickness of the material.

Noting that t is larger than d, we can conclude that ligament buckling will occur in the plane of the lattice, as opposed to out of plane. The ligament has an approximate moment of inertia

$$I = \frac{td^3}{12} \tag{7}$$

Therefore, from equation (6), P_{cr} will be proportional to

$$P_{cr} \propto \frac{I}{L^2} \quad \text{or} \tag{8a}$$

$$P_{cr} \propto \frac{td^3}{L^2} \tag{8b}$$

The corresponding critical stress, $\sigma_{cr} = \frac{P_{cr}}{A}$, where the cross-sectional area of the ligament is $A = td$, will be proportional to

$$\sigma_{cr} \propto \left(\frac{d}{L}\right)^2 \tag{9}$$

With the square lattice, one long, continuous column of a series of pinned-pinned columns is formed down the length of the specimen. As small loads are applied to the specimen, the material and structure deforms in a linear elastic way and the ligaments uniformly compress. At some critical load however, the ligaments will buckle. The nominal stress of the overall structure will remain constant as the strain increases and energy is used in deformation.

In the hexagonal lattice, the ligaments are interrupted at every row, and a continuous series of columns is not formed. This results in only very short constrained columns that are not directly axially loaded. In this lattice buckling is not favorable, and instead shear forces act to initiate an instability. At small compressive loads linear elastic behavior is seen as with the square lattice. However, at larger loads the position becomes unstable, and shear deformation occurs, resulting in a nonlinear elastic behavior of the structure.

The inclusions introduced into the voids of the lattice provide an added stiffness to the buckling analysis. When the voids are empty, there are no external lateral restraining forces on the column that restrain buckling. The buckling depends entirely on the properties of the column, boundary conditions, and the compressive load. With the addition of inclusions into the voids there are now restraints on the lateral movement, and therefore on the buckling of the column. The inclusions have some stiffness associated with them, and can be modeled as springs on the sides of the column.

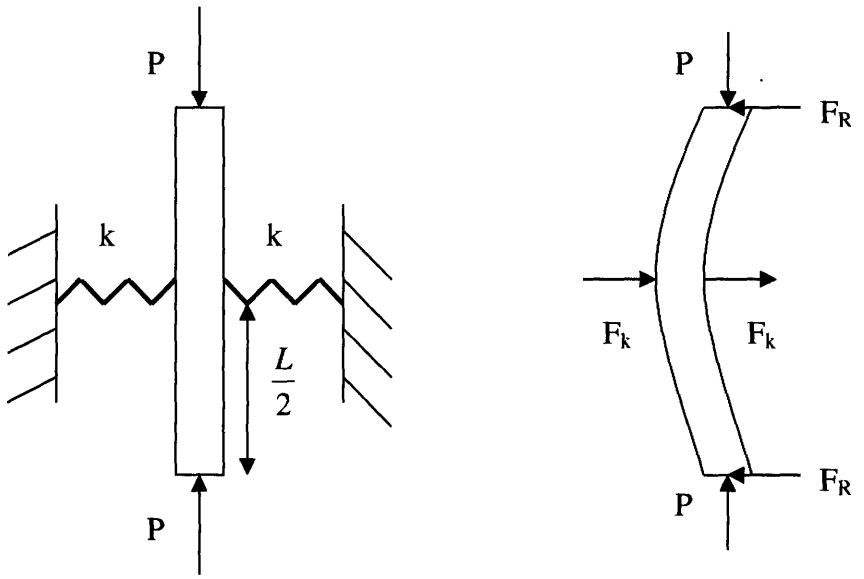

Figure 4: Column with lateral springs of stiffness k

The springs work to stabilize the bar by exerting a restoring force on the column. If the column is moved some small horizontal distance y, the springs will exert a force of magnitude

$$P_k = 2ky \tag{10}$$

on the column. The ligaments next to voids with inclusions will therefore require a larger force to buckle than voids without inclusions.

In the case of a lattice with both voids and inclusions, when the rows of inclusions are perpendicular to the compression axis, once the domains with voids buckle, the stress on the lattice remains constant, and the domain with inclusions will not buckle because their overall critical load will not be reached. When the domains with inclusions are coaxial with the compression direction, they will require a larger strain and stress to buckle than the voided domain; hence the voided domains will buckle first and the domains with inclusions will transform at a larger stress. These results imply that the holes with inclusions will not have a pattern transformation triggered along with all of the voids that remain empty. This suggests that we can create preferential patterns of transformation versus non-transforming domains.

The material properties of the inclusions can be changed in order to differ the effects on the pattern transformation. Inclusions with different stiffnesses will apply different magnitude forces on the ligament beams. Higher stiffnesses will prevent any buckling of the ligament, while lower stiffnesses will allow the ligament to buckle and the holes with inclusions to have some pattern transformation.

2.2 Detailed Finite Element Model of the Structure

The above ligament buckling analysis is only an approximation of the actual behavior of the lattice as a whole. In order to more accurately model the behavior of the material, with and without inclusions, finite element analysis is used. The finite element method is utilized to determine the stresses in a system by creating a mesh of finite-sized

elements of the overall geometry of the system. Appropriate material properties and boundary conditions are applied, and the stresses and strains in the system are calculated.

For the lattices described above, the nonlinear finite element code ABAQUS was used to evaluate the stresses, strains, and deformations of the material. The geometry of the lattice was reproduced as a 2D planar structure. The mesh was made of 6-node, quadratic, hybrid, plane strain elements (ABAQUS element type CPE6H). The analysis was done considering the whole specimen, and applying appropriate boundary conditions. The bottom edge is fixed in the vertical direction, and the bottom left corner is fixed in the horizontal direction to prevent any rigid body motion. The top edge of the specimen is uniformly compressed in the vertical direction.

The inclusions are modeled with the same elements as the lattice material, but different material properties. The boundary between the inclusions and the lattice is assumed to be perfect contact, so that there is no movement of the inclusion along the surface of the lattice. A linear elastic model is used for the inclusions, with a shear modulus of 0.10 MPa and a Poisson's ratio of 0.3.

The elastomeric sheet used to construct the lattices does not behave in a small strain linear elastic way. The material is instead modeled with the neo-Hookean large strain elastic model. This rubber elastic model assumes an initially small shear modulus G, but an initially large bulk modulus K. The initial Poisson's ratio will then be

$$\nu = \frac{1 - \frac{2G}{3K}}{2 + \frac{2G}{3K}}. \tag{11}$$

With a shear modulus three orders of magnitude less than the bulk modulus, $\upsilon = .4995$. The material is therefore nearly incompressible. Shape change will occur easily due to the small shear modulus, but the there will be little to no volume change with deformation. The material is modeled in the finite element analysis as a nearly incompressible neo-Hookean material with a shear modulus of 3.9 MPa and a Poisson's ratio of 0.499.

The finite element analysis is used to measure key values of the system under a compressive load. The nominal stress versus nominal strain behavior of the structure is determined by measuring the total force on the bottom edge of the lattice as a function of the applied displacement. The nominal strain is found with the expression

$$\varepsilon = \frac{dL}{L_0} \tag{12}$$

where dL is the change in length and L_0 is the original length of the structure. For the numerical analysis the applied displacement is divided by the original length of the specimen. The nominal stress is then found

$$\sigma = \frac{P}{A_0} \tag{13}$$

where P is the axial force on the specimen, and A_0 is the original area of the top surface of the specimen. The nominal stress versus nominal strain curves can then be constructed from these values.

In order to preferentially initiate the desired mode of buckling, several imperfections were placed within the mesh.

The deformation of the specimen is also visualized using ABAQUS. The Mises stress, a function of the overall stress tensor, gives a scalar equivalent measure of the stress

$$\sigma_v = \sqrt{\frac{(\sigma_1 - \sigma_2)^2 + \sigma_2^2 + \sigma_1^2}{2}} \tag{14}$$

A color contour plot of the Mises stress is also calculated in order to visualize the stress distribution within the specimen under compression.

3. Experimental Methods

Specimens were water jet cut from sheets of a photoelastic polymer PSM-4 (Measurements Group). Circular holes were cut into the material in either a square or hexagonal lattice.

Specimen 1: 117 mm by 115.4 mm and 9.75 mm thick, with a square array of circular holes. The diameter of each hole is 8.89 mm, with a vertical and horizontal center to center spacing of 10.49 mm. This results in a ligament thickness between each hole of 1.6 mm. The last hole on each side of each row is a semicircle that opens on the edge of the piece. This results in 11 rows, and 10 columns plus two semicircular columns of holes.

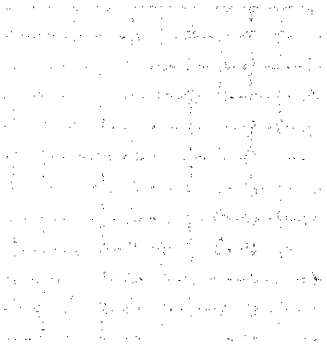

Specimen 2: 117.1 mm by 111 mm and 9.75 mm thickness, with a hexagonal array of circular holes. The diameter of each hole is 8.89 mm, with a vertical and horizontal center to center spacing of 10.49 mm. This results in a ligament thickness between each hole of 1.6 mm. The last hole of every other row on both sides is a semicircle that opens on the edge of the piece. This results in 11 rows with 10 holes plus one half-circle in each row.

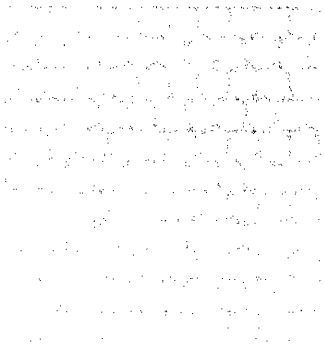

The specimens were tested under uniaxial compression using a Zwick screw-driven machine. The specimens were placed between two 5 mm thick polymethylmethacrylate (PMMA) sheets, which were both lightly dusted with chalk to reduce friction. The sheets help to stop any out of plane buckling. The specimen and PMMA sheets were then placed in a trough approximately 20 mm wide and 10 mm high in order to secure the set up at the bottom in an upright orientation, shown in Figure 5.

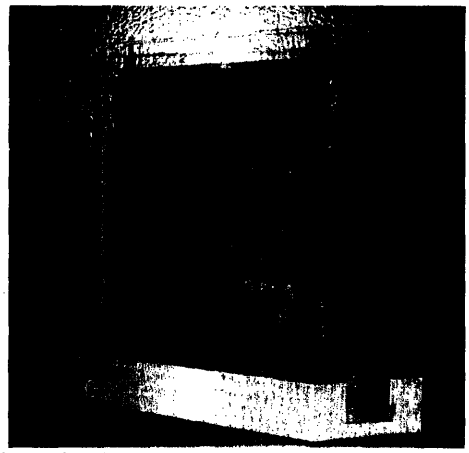

Figure 5: Lattice and PMMA sheets held at bottom in trough

The specimen was compressed from the top by an aluminum bar that lay across the entire width of the specimen, therefore uniformly displacing the top. The Zwick machine compressed the specimen at a rate of 10 mm/min in a cyclic pattern with one cycle consisting of a load followed by an unload. A photograph of the specimen was taken every 0.01 strain, with a Q-Imaging Retiga 1300 camera with a 200 mm lens.

Inclusions were then introduced into the holes of the specimens. The inclusions were composed of cotton balls, which could be placed in specified voids in varying densities. For each test, the density of cotton balls in all of the holes with inclusions was kept approximately the same. The density was then varied uniformly for all of the inclusions.

The inclusions were added in several different patterns in order to induce different pattern changes in the overall specimen:

Vertical Inclusions: The inclusions are inserted in the center two columns of the specimen.

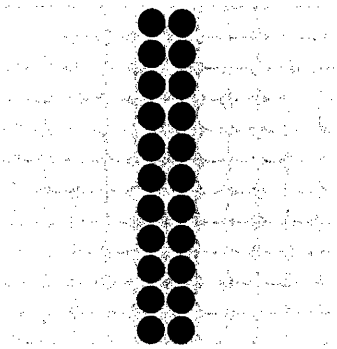

Horizontal Inclusions: The inclusions are inserted into the center row of the specimen.

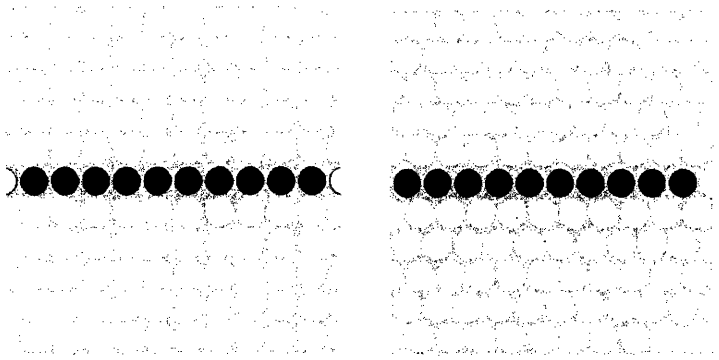

Cross Inclusions: The inclusions are inserted into both the center row and columns of the specimen.

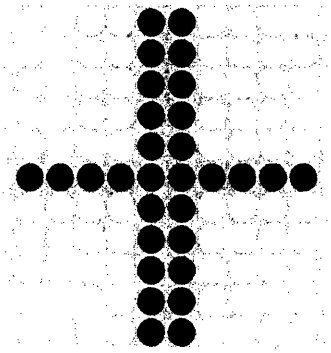

4. Results and Analysis

The results of both the experimental tests and ABAQUS analysis are presented below. Both the square and hexagonal lattices are shown with various patterns of inclusions.

4.1 Square Lattice

4.1.1 No Inclusions

The results of the nominal stress versus nominal strain are shown in Figure 6. Initially, under an axial compressive load the structure exhibits linear elastic behavior. The stress then hits a peak, and reaches a plateau where stress does not change with increased strain. The plateau occurs with the triggering of the pattern change. The curve also shows some hysteresis which may be caused by friction between the specimen and the PMMA sheets.

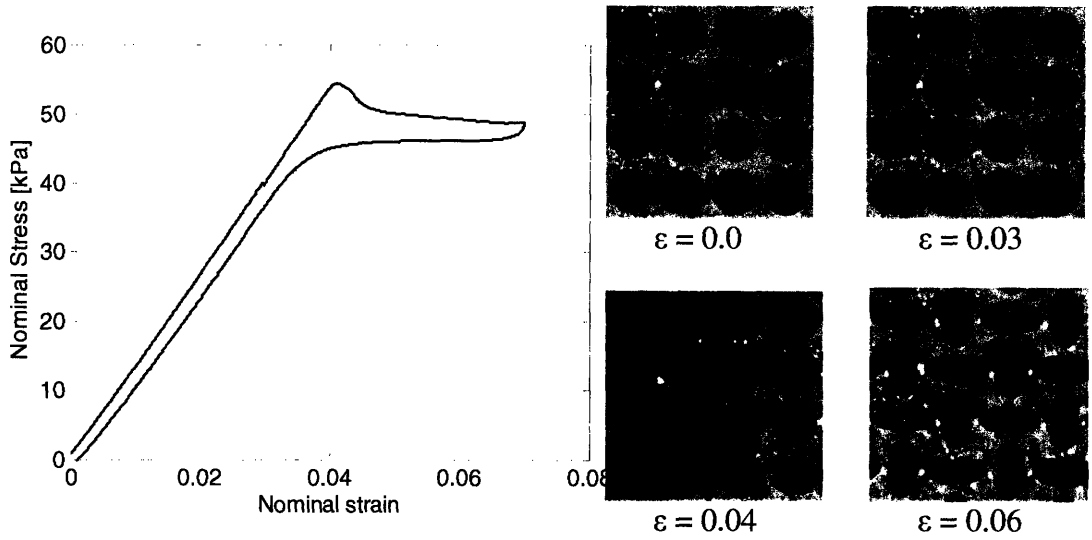

Figure 6: 1) Nominal Stress versus Nominal Strain of Square Lattice, No Inclusions. 2) Experimental images of lattice at 0%, 3%, 4%, and 6% nominal strain

The voids in the lattice undergo uniform compression during the linear elastic regime of the stress-strain curve. At the start of the plateau, the pattern change is triggered, and the shapes of the holes change significantly. A pattern of ellipses in alternating orthogonal directions is formed. As the strain increases the ellipses are further stretched, with the length of the major axis increasing, and the length of the minor axis decreasing.

The stress-strain behavior of the specimen is also determined numerically with finite element analysis. The agreement between the numerical and experimental results is seen in Figure 7.

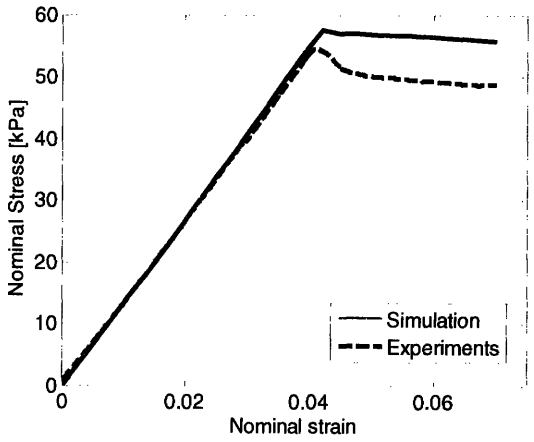

Figure 7: 1) Nominal Stress versus Nominal Strain of Square Lattice, No Inclusions, Numerical and Experimental

The agreement between the simulations and experiments in the linear elastic regime is excellent. However, the load at which the pattern change is triggered and buckling begins is higher in the numerical results. The difference may be due to some discrepancy in the dimensions used in the model and the exact dimensions of the

specimen. It could also be due to the nature of the real imperfections and the imperfections in the model.

There is also excellent qualitative agreement between the images of the numerical and experimental results. The uniform compression of the voids as well as the pattern change and subsequent lengthening of the ellipses are captured by the images from both sets of results as shown in Figure 8.

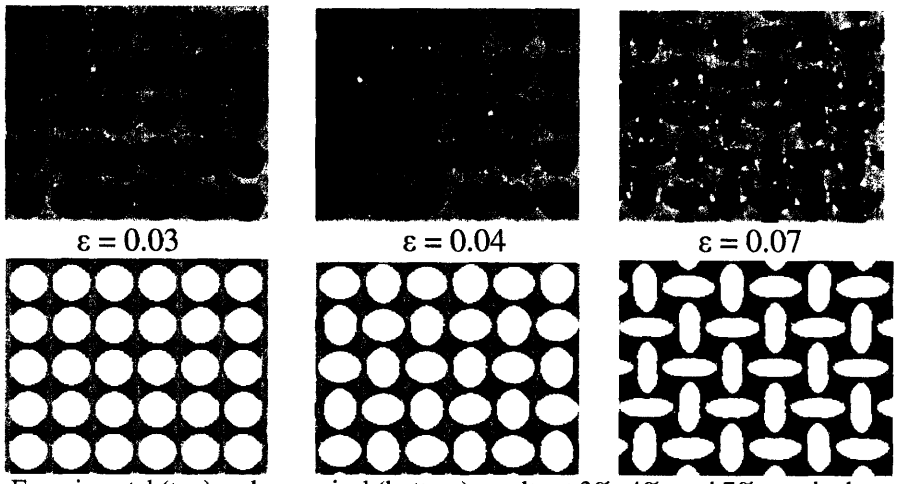

Figure 8: Experimental (top) and numerical (bottom) results at 3%, 4%, and 7% nominal strain. At 3% strain the voids are uniformly compressed, at 4% strain the pattern is triggered, and at 7% strain the pattern is more accentuated.

The nearly full views of the specimen seen in Figure 9 once again show excellent agreement between the experimental and numerical results, even at the edges where the boundary conditions affect the deformation.

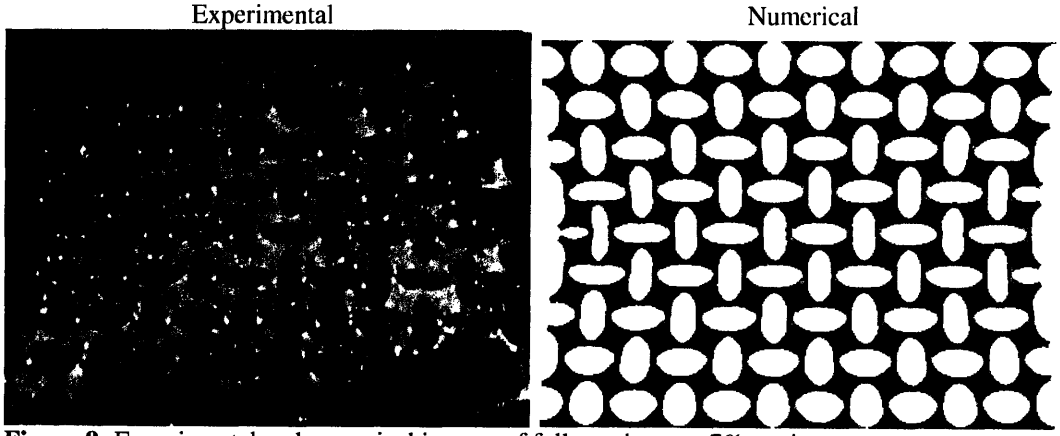

Figure 9: Experimental and numerical images of full specimen at 7% strain

The finite element analysis also provides a buckling analysis of the different modes of buckling that the material can undergo. Using a linear perturbation procedure, the finite element code ABAQUS calculates the buckling load.

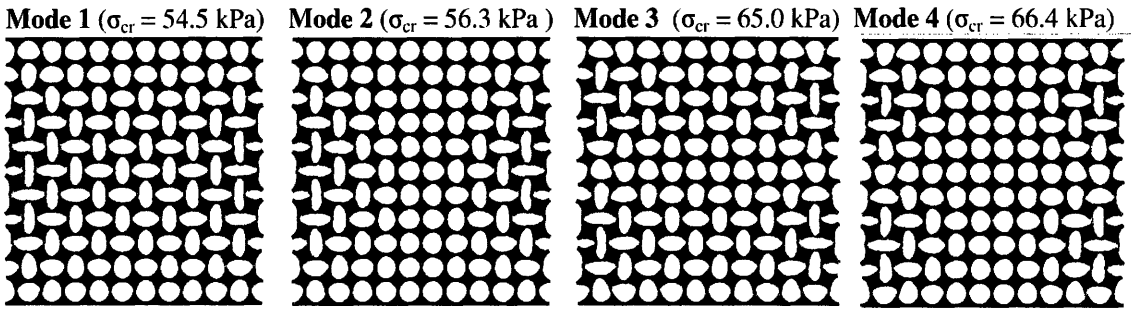

Figure 10: First four buckling modes of square lattice, and the critical stresses at which buckling occurs

The first four buckling modes show four distinct pattern changes that all occur at different critical buckling loads. With no inclusions only the first buckling mode is seen because it requires the lowest stress to initiate the pattern change.

Overall there is good agreement between the experimental and the model numerical results. The same pattern change is seen in the numerical model and the experimental results, and is seen homogeneously throughout the material, with the exception of the boundary layer of voids at the top and bottom surfaces which are constrained by the interaction with the loading platens.

4.1.2 Vertical Inclusions

In order to suppress mode one in favor of mode two of the buckling analysis, vertical inclusions are placed in the lattice. The inclusions used had a shear modulus of about 0.10 MPa and a Poisson's ratio of 0.3. The nominal stress versus nominal strain is shown below in Figure 11.

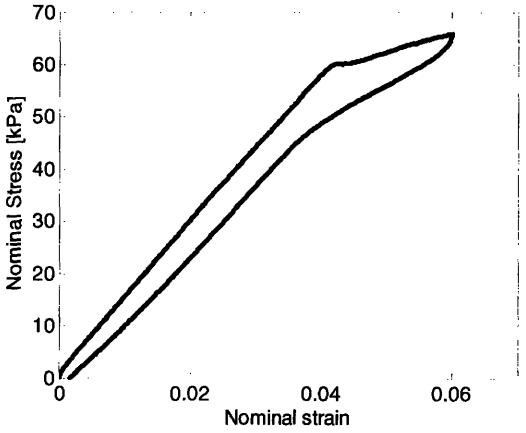

Figure 11: Nominal Stress versus Nominal Strain of Square Lattice, Vertical Inclusions

At lower strains the material once again shows linear elastic behavior. After the critical buckling load is reached however, the behavior differs from the case with no inclusions. Instead of reaching a plateau there is a decrease in slope. This behavior is seen because the inclusions are still being compressed. After the pattern change is triggered, all of the increase in stress is a result of the compression of the inclusion domains, where the transformed voided region is now in its load plateau response and no longer

contributes to the specimen stiffness. This is somewhat analogous to three springs in parallel where two of the springs are the lattice with voids and the third spring is the lattice with inclusions. The stress that initiates buckling of the structure with vertical inclusions is higher than that required for the corresponding lattice with no inclusions. A higher overall buckling stress is also seen in the onset of the mode two pattern transformation of the lattice with no inclusions.

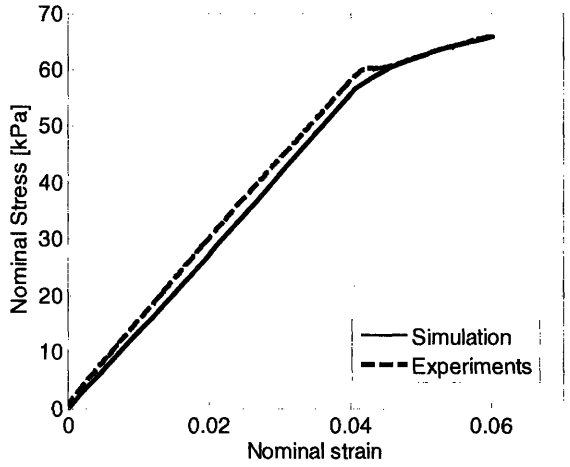

Figure 12: Nominal Stress versus Nominal Strain of Square Lattice, Vertical Inclusions, Numerical and Experimental

The numerical and experimental results for the stress-strain behavior of the material have excellent agreement, as shown in Figure 12. Both the predicted initial linear elastic regime and the regime after buckling are in good agreement with the experimental data. The critical load at which buckling is initiated is very close in both results.

The qualitative agreement between the images from both the numerical and experimental results is also very good, as shown in the deformation sequences of Figure 13.

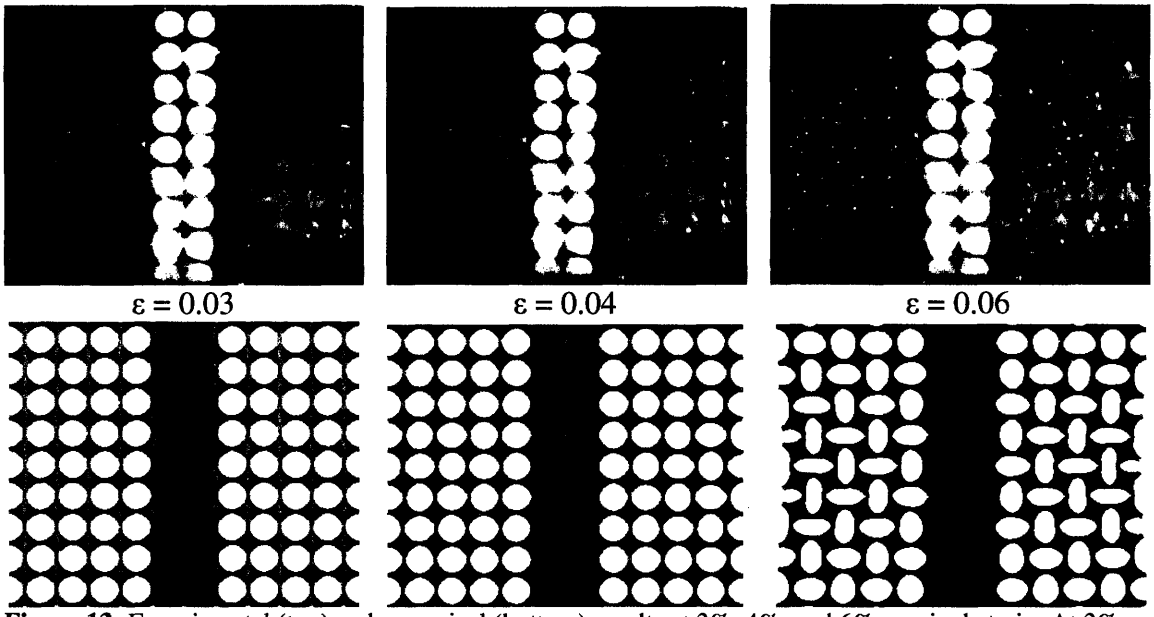

Figure 13: Experimental (top) and numerical (bottom) results at 3%, 4%, and 6% nominal strain. At 3% strain the voids are uniformly compressed, at 4% strain the pattern is triggered, and at 6% strain the pattern is more accentuated.

Both the pattern of alternating direction ellipses, as well as the overall pattern induced by the inclusions can be seen in the experimental and numerical results. While the lattice with no inclusions shows a homogeneous pattern change throughout the structure, with vertical inclusions there are distinct regions in which the pattern change occurs. The ellipses are more accentuated in a triangular region on either side of the columns of inclusions. Outside of this triangular region, the ellipses begin to widen, and are closer to the original circular form the farther from the region they are located. These results demonstrate an ability to pattern the transforming regions.

This triangular pattern observed in the lattice with vertical inclusions closely matches the second buckling mode found in the lattice with no inclusions (Figure 14).

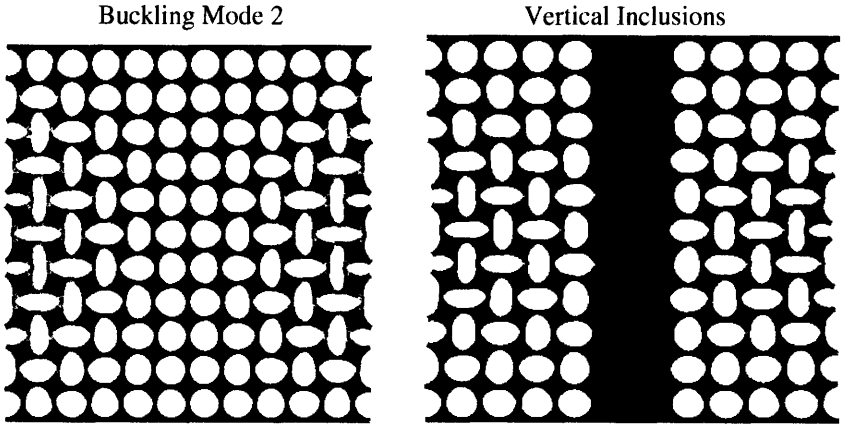

Figure 14: 1)Second buckling mode found using finite element analysis with no inclusions. 2) Lattice with vertical inclusions at 6% nominal strain

The buckling mode two and lattice with vertical inclusions are a close match, but there are differences between the two. While the buckling mode is perfectly symmetric about

the vertical axis, the lattice with inclusions is not. The center two columns of mode two have the voids as mirror images of each other, whereas with the inclusions the center columns have the ellipses pointing in orthogonal directions, as seen in Figure 15. This asymmetry results in opposite sides of the lattice having ellipses that are orthogonal to each other instead of being symmetric.

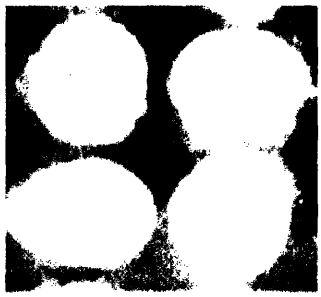

Figure 15: Inclusions deform in asymmetric directions

Although the lattice with horizontal inclusions does not exactly mimic the second buckling mode of the inclusion-free lattice, it is still very similar. The overall triangular pattern of accentuated ellipses is seen in both cases. These results show that by suppressing the first buckling mode with the introduction of inclusions, the second buckling mode can be seen. A specified pattern transformation is achieved through the use of strategically placed inclusions into the lattice. The pattern transformation was predictable both by examining the buckling modes of the inclusion-free lattice as well as through finite element analysis of the lattice with the specified inclusions.

4.1.3 Horizontal Inclusions

The stress-strain behavior of the square lattice with horizontal inclusions (Figure 16) follows closely with that of the lattice with no inclusions. Initially the curve exhibits linear elastic behavior, then reaches a plateau stress when the pattern change is initiated.

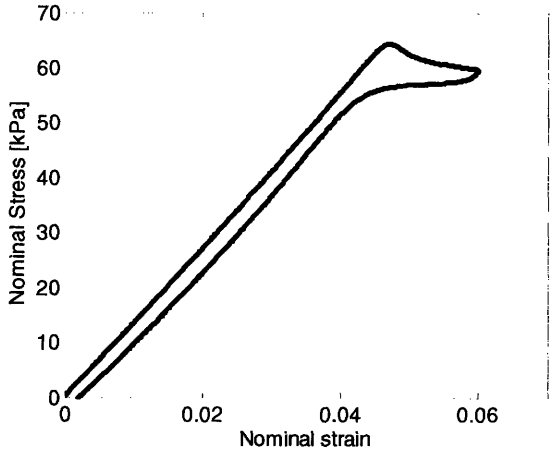

Figure 16: Nominal Stress versus Nominal Strain of Square Lattice, Horizontal Inclusions

While the overall shape of the curve is very similar to the case with no inclusions, the critical stress required to initiate the pattern change is higher. This slightly higher critical

strain is a result of the inclusions providing an additional boundary layer effect on the initiation of the instability, similar to the top and bottom surface.

Figure 17 shows that the numerical and experimental results for the stress-strain behavior of the lattice with horizontal inclusions are in good agreement. The initial linear elastic regimes are very similar for both results. As with the case with no inclusions, the critical stress is slightly higher in the numerical model than the experimental results.

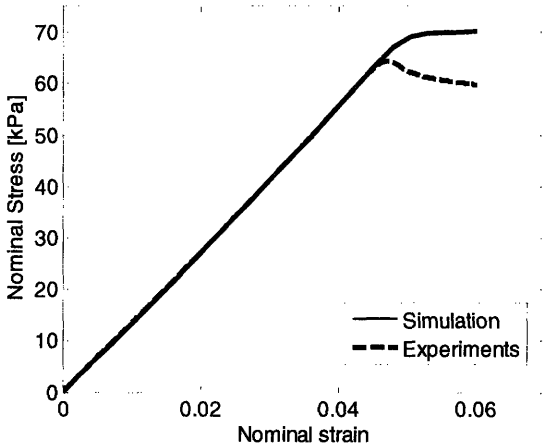

Figure 17: Nominal Stress versus Nominal Strain of Square Lattice, Horizontal Inclusions, Numerical and Experimental

The agreement between the images of the numerical and experimental results, however, is not as close. (Figure 18)

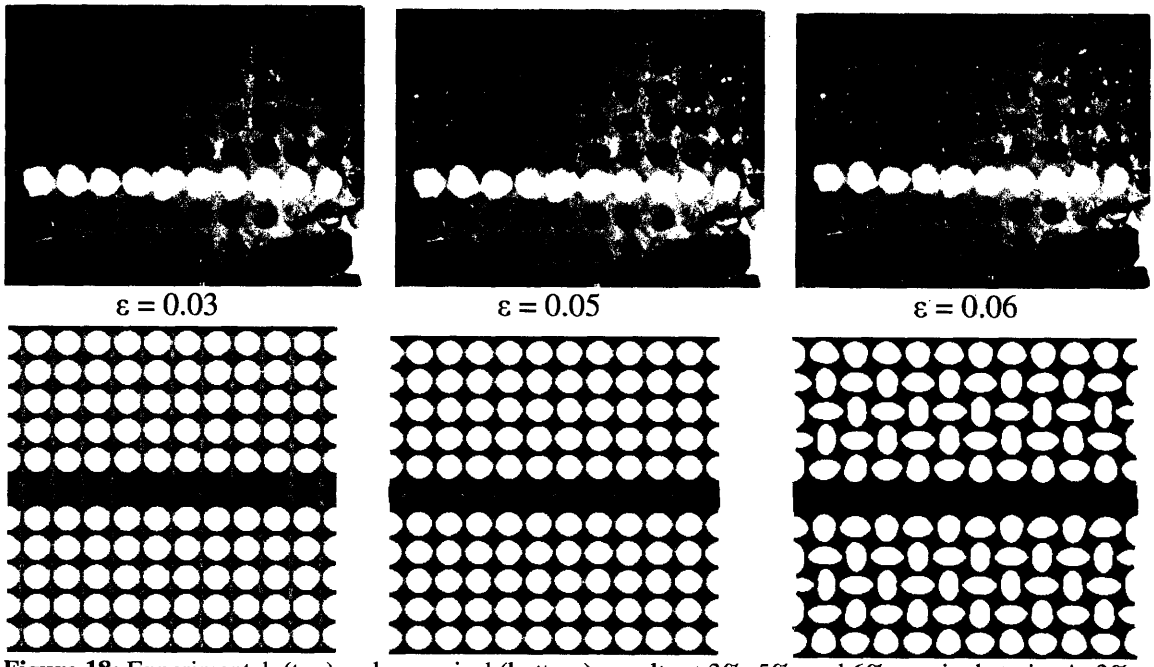

Figure 18: Experimental (top) and numerical (bottom) results at 3%, 5%, and 6% nominal strain. At 3% strain the voids are uniformly compressed, at 5% strain the pattern is triggered, and at 6% strain the pattern is more accentuated.

While the numerical model shows symmetric pattern transformation on either side of the row of inclusions, the experimental results show pattern transformation only being triggered on one side of the row of inclusions. Instead of merely suppressing the pattern change at the row of inclusions, the inclusions act as a barrier that prevents the pattern from being triggered on the other side. The triggering on one side of the inclusions is due to the fact that the system is not truly symmetric in the experimental setup. The material is being held at the bottom between the PMMA sheets, and so the very bottom of the structure is not as free to deform as the rest of the lattice is. The pattern transformation is therefore triggered preferentially at the top of the specimen where there are less constraints. Once the pattern change is triggered on one side, the stress reaches a plateau, and so the pattern change will not be triggered on the bottom half, where a higher critical stress is required. Any increased strain works to further accentuate the pattern of ellipses on the top half. In the numerical model everything is symmetric, and so the pattern is triggered at the same critical stress on both sides of the row of inclusions.

In practice it may be difficult to produce truly symmetric boundary conditions. With this stiffness of inclusions it may therefore be difficult to trigger the pattern change on both sides of the inclusions. A much larger lattice will lessen the effects of the boundary conditions, and may be more likely to allow triggering of the pattern change on both sides of the row of inclusions.

While the experimental results do not yield a pattern similar to the third buckling mode of the lattice with no inclusions, the numerical model does show this pattern.

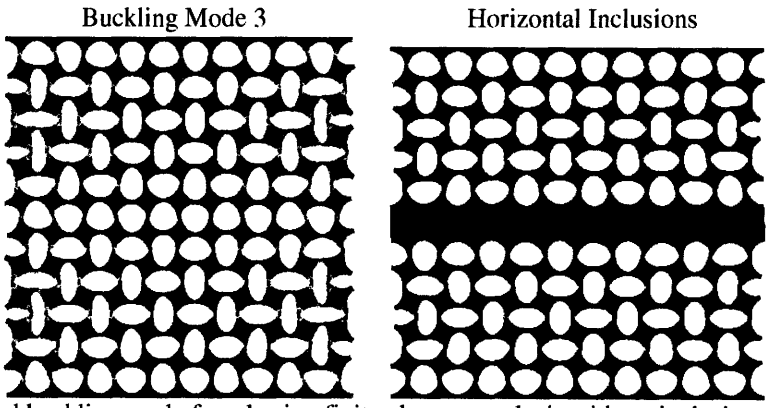

Figure 19: 1) Third buckling mode found using finite element analysis with no inclusions. 2) Lattice with horizontal inclusions at 6% nominal strain

Figure 19 shows that the pattern transformation seen in the numerical model of the lattice with horizontal inclusions closely follows that of the third buckling mode of the inclusion-free lattice. This result indicates that the third buckling mode can be reproduced by suppressing the first buckling mode. If a more symmetric experimental setup can be produced, the third buckling mode may also be preferentially triggered in experiment.

4.1.4 Cross Inclusions

The stress-strain behavior of the square lattice with cross inclusions is seen below in Figure 20.

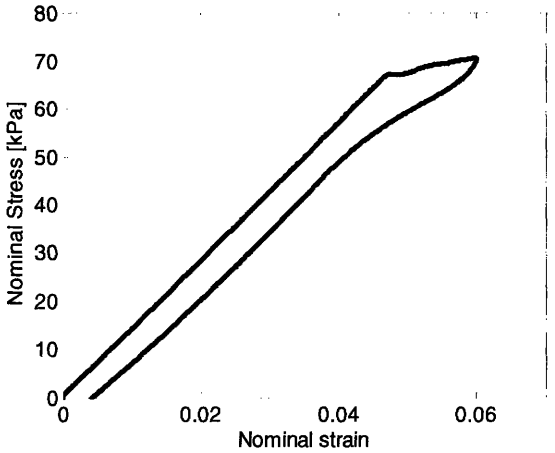

Figure 20: Nominal Stress versus Nominal Strain of Square Lattice, Cross Inclusions

The behavior is similar to that of the lattice with only vertical inclusions. The initial behavior follows a linear elastic pattern, and after the pattern change is initiated, a lower slope is followed. This second regime is once again the result of the vertical inclusions being compressed even after the pattern change starts in the rest of the lattice. The stress at which buckling is initiated is higher than any of the previous cases, which is consistent with the higher critical buckling load of the fourth buckling mode of the lattice with no inclusions.

The agreement between the numerical and experimental results is seen Figure 21. Both the initial linear elastic region and the critical buckling stress is very similar in both results. There is a slight difference in the slopes of the curves after the critical stress is reached, which may be due to some discrepancy between the properties of the model and the experiment.

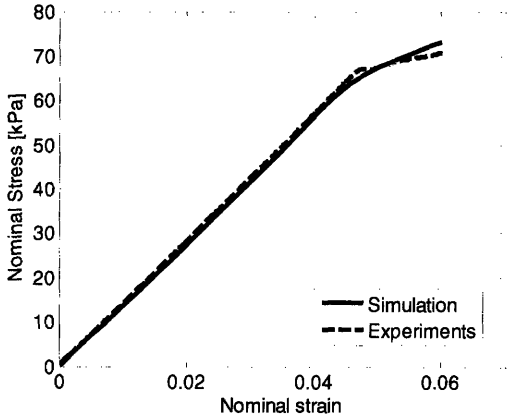

Figure 21: Nominal Stress versus Nominal Strain of Square Lattice, Cross Inclusions, Numerical and Experimental

Similar to the case with just horizontal inclusions, in the experimental results the pattern is not triggered below the row of horizontal inclusions. Because of the asymmetry of the boundary conditions, the pattern change is preferentially triggered in only the top rows of the lattice, and the bottom rows remain circular voids. The horizontal row of inclusions acts as a barrier to prevent the pattern from being triggered below them.

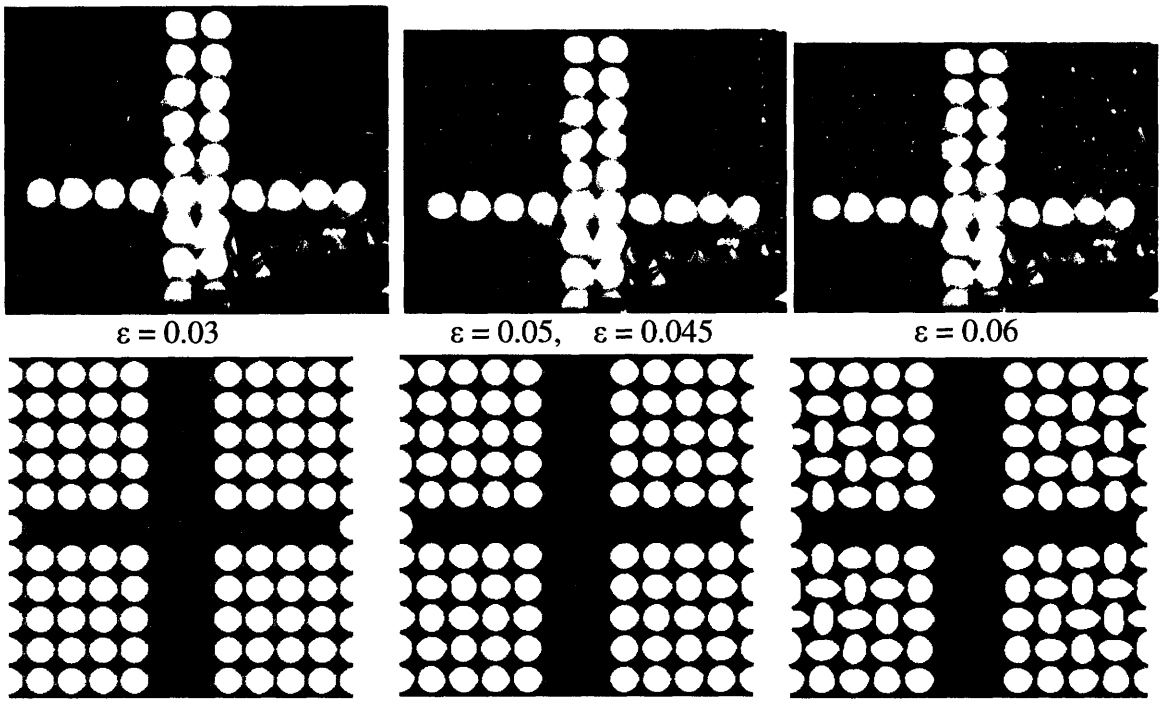

Figure 22: Experimental (top) and numerical (experimental) results at 3%, 5% for experimental and 4.5% for numerical, and 6% nominal strain. At 3% strain the voids are uniformly compressed, at 5% strain the pattern is triggered, and at 6% strain the pattern is more accentuated.

The cross inclusions demonstrate another effect of asymmetry on the pattern transformation.

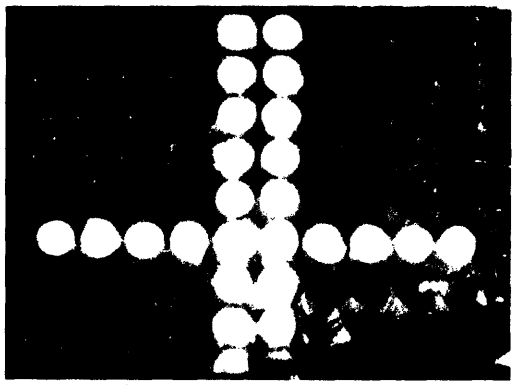

Figure 23: Experimental image at 5% nominal strain, pattern transformation triggered on only left side of lattice

Figure 23 shows that the pattern change is first triggered in one quadrant of the lattice, and the pattern change in the other top quadrant follows later. This result shows that any asymmetry in the material or inclusions can lead to preferential triggering of the pattern change in a small localized area of the specimen. The pattern transformation does occur in the other half with increased strain, showing that vertical inclusions do not act as a barrier to pattern transformation in other areas of the lattice than where it first occurs.

4.1.5 Combining Cases

The stress-strain behavior of the lattice with no inclusions, as well as with the three different patterns of inclusions is shown below (Figure 24).

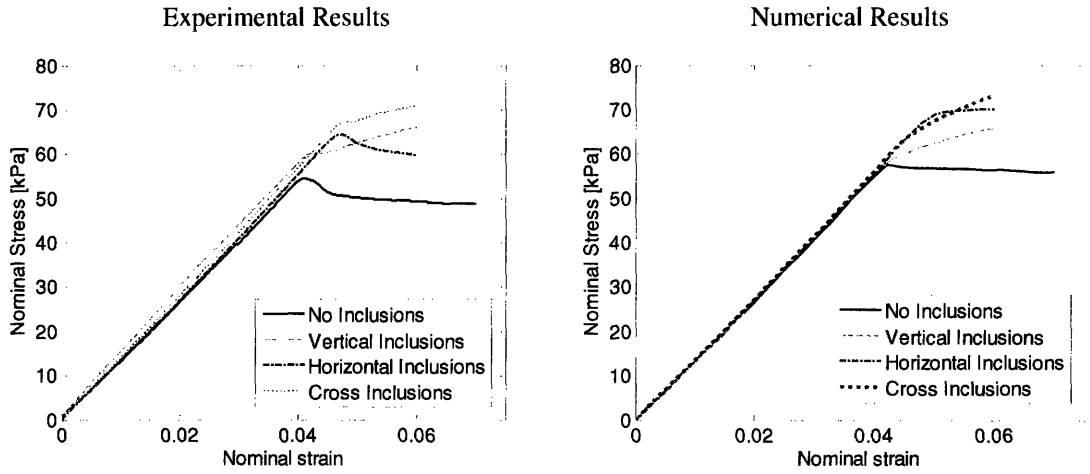

Figure 24: Nominal Stress versus Nominal Strain of Square Lattice, Experimental and Numerical Results, all cases of inclusions

The linear elastic regime remains the same in all cases, with slight variations in slope due to the addition of the stiffness of the inclusions. The critical buckling load at which the pattern transformation is triggered is different for each case. In the experimental results, the load for the case with no inclusions is the lowest, while the load increases for the cases with vertical, horizontal, and cross inclusions, respectively. The order in which the load increases follows the order of the buckling mode that each case is trying to mimic. With the numerical results, the horizontal inclusions show the highest critical stress value. Both the vertical and cross cases show a non-zero slope after buckling occurs that results from the ongoing stiffness contribution from the compression of the inclusions.

4.2 Hexagonal Lattice

4.2.1 No Inclusions

The pattern transformation in the hexagonal lattice is triggered by local shear instability due to shear in the ligaments diagonally bridging the voids as opposed to the buckling instability seen in the square lattice. The stress-strain behavior therefore shows different qualities.

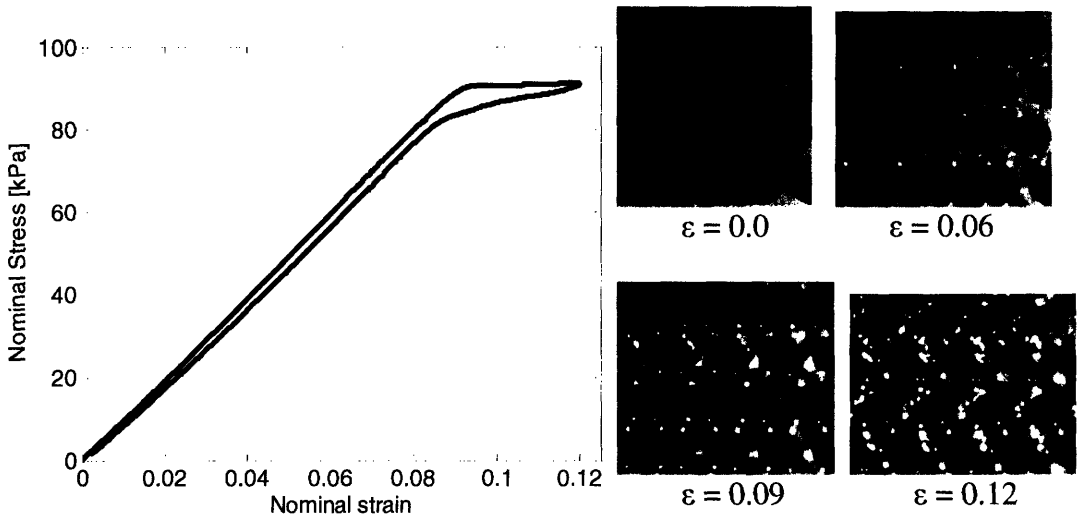

Figure 25: 1) Nominal Stress versus Nominal Strain of Hexagonal Lattice, No Inclusions. 2) Experimental images of lattice at 0%, 6%, 9%, and 12% nominal strain

The overall shape of the stress-strain behavior for the hexagonal lattice is the same as that of the square lattice. Initially it shows linear elastic behavior, and then reaches a plateau stress at the initiation of the pattern transformation. Some hysteresis is seen in both cases. However, there are a few key differences between the square and hexagonal structures. The hexagonal lattice curve in the linear elastic regime is less stiff than the square lattice. This difference is due to the orientation of the ligaments in the lattice. In the square lattice the ligaments line up on top of each other, resulting in one long column the length of the specimen. In the hexagonal lattice, each ligament is bordered on either end by a void, so no long column is observed. These shorter columns result in a lower stiffness of the overall lattice. Another difference between the two lattices is the critical load at which the pattern transformation is triggered. The load is considerably higher with the hexagonal lattice. This higher load is a result of the different types of instability that trigger the pattern transformation. The shear instability seen in the hexagonal lattice requires a higher load to initiate.

The agreement between the numerical and experimental stress-strain curves is seen below in Figure 26.

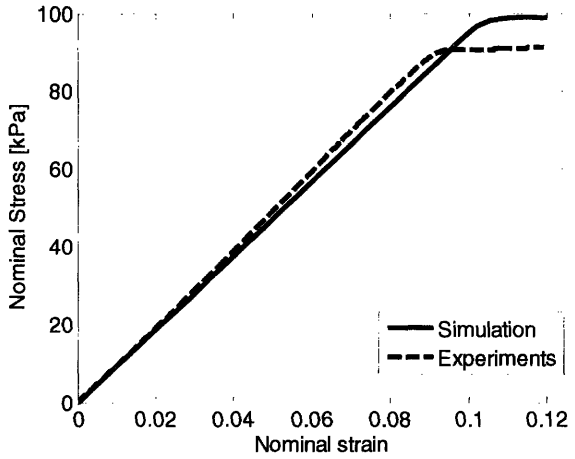

Figure 26: Nominal Stress versus Nominal Strain of Hexagonal Lattice, No Inclusions, Numerical and Experimental

As with the square lattice, the agreement in the linear elastic regime is good, but the critical load required to initiate the pattern transformation is higher for the simulations than the experiments. The discrepancy may once again be due to some inconsistency between the actual size of the specimen and the dimensions used in the model or the difference between the real imperfections and the imperfections placed in the model.

The pattern change seen in the hexagonal lattice is distinct from the pattern seen in the square lattice. Initially the voids undergo uniform compression, as with the square lattice. Because of the higher critical stress, the voids are compressed further than observed with the square lattice, and begin to flatten out at the top and bottom. Once the shear instability is triggered, the voids form alternating direction sheared rows. The pattern change is seen homogeneously throughout the lattice.

The qualitative agreement between the images captured during the experiments and the numerical analysis is once again very good. The pattern of alternating sheared voids is captured in both cases.

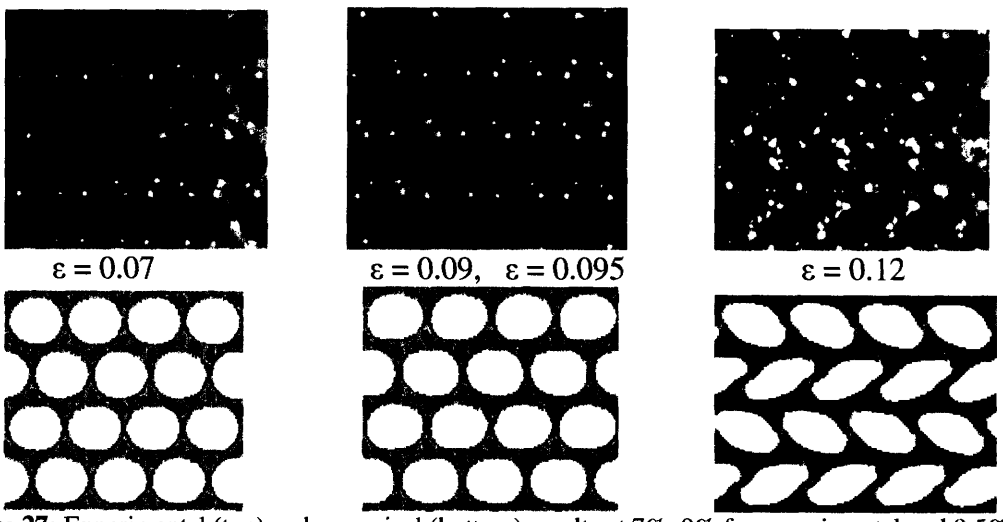

Figure 27: Experimental (top) and numerical (bottom) results at 7%, 9% for experimental and 9.5% strain for numerical, and 12% nominal strain. At 7% strain the voids are uniformly compressed, at 9% strain the pattern is triggered, and at 12% strain the pattern is more accentuated.

Nearly full views of the experimental and numerical results also display excellent qualitative agreement. The effects at the boundary conditions are captured in both cases.

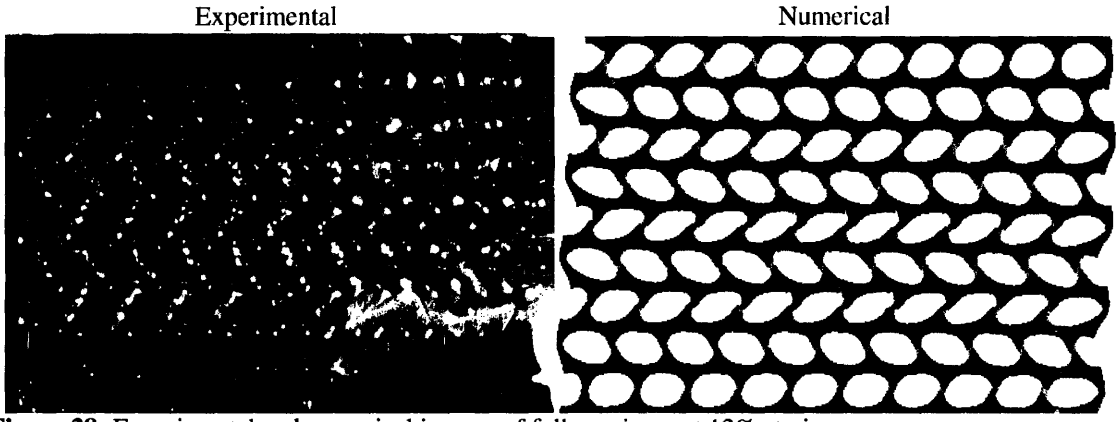

Figure 28: Experimental and numerical images of full specimen at 12% strain

The first four buckling modes and their associated critical buckling stresses are also found with finite element analysis (Figure 29).

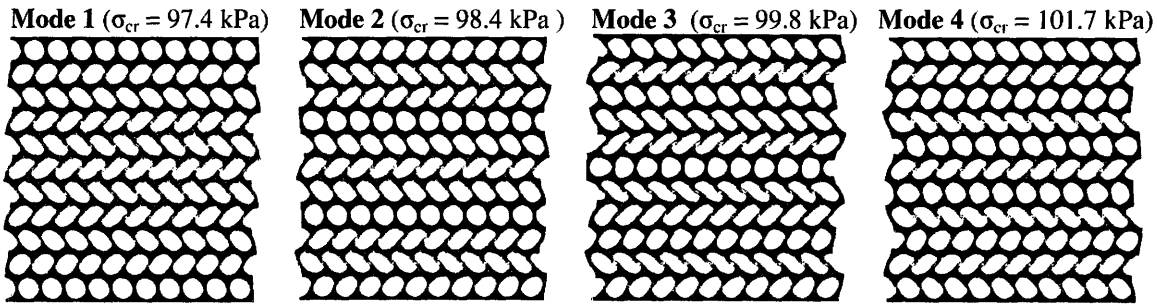

Figure 29: First four buckling modes of hexagonal lattice

Only the first mode is seen in the case with no inclusions. This mode requires the lowest critical stress, and is therefore preferentially initiated. However, the critical stress required for mode two is only 1% greater than that for mode one.

Overall the agreement between the experimental and numerical results for the hexagonal lattice is good. The stress-strain behavior as well as the shape of the deformation after pattern change seen in the experimental results are captured by the numerical model.

4.2.2 One Row of Horizontal Inclusions

The stress-strain behavior for the hexagonal lattice with one row of horizontal inclusions (Figure 30) is very similar to the behavior seen with no inclusions (Figure 26).

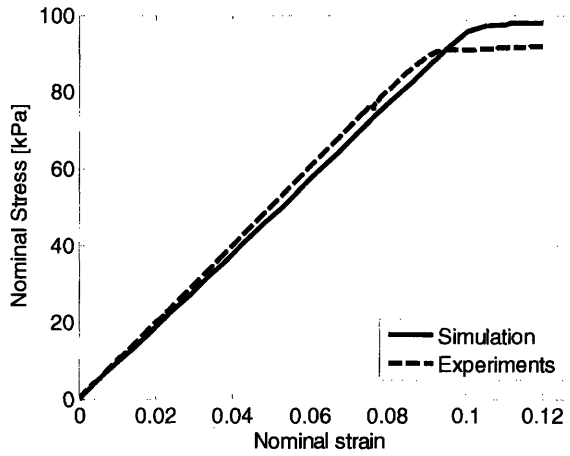

Figure 30: Nominal Stress versus Nominal Strain of Hexagonal Lattice, One Row Horizontal Inclusions, Numerical and Experimental

The critical stress value where the plateau begins is very close to the value found in the lattice with no inclusions. This similarity is true for the both the experimental and numerical results. These results are consistent with similarity in critical buckling stress for mode one and mode two found in the buckling analysis.

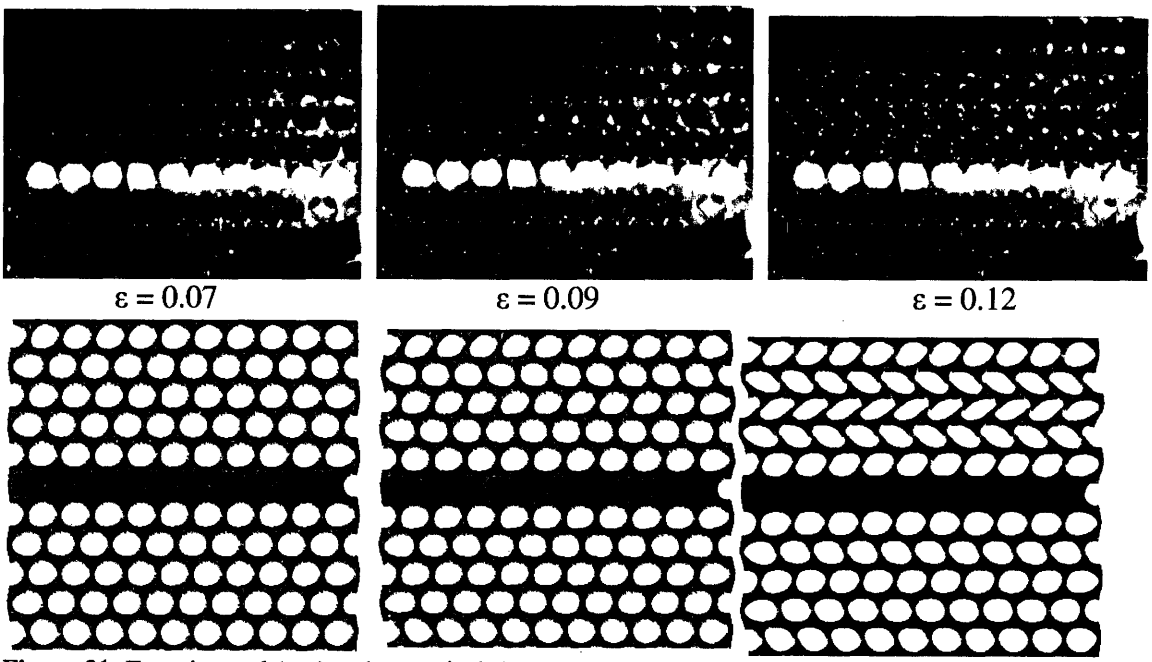

Figure 31: Experimental (top) and numerical (bottom) results at 7%, 9%, and 12% nominal strain. At 7% strain the voids are uniformly compressed, at 9% strain the pattern is triggered, and at 12% strain the pattern is more accentuated.

As with the horizontal inclusions in the square lattice, the pattern change only takes place above the row of inclusions. The inclusions act as a barrier to triggering of the pattern change. The set up is once again asymmetric, resulting in a higher critical stress needed to initiate shearing in the lower half of the lattice.

Unlike the numerical results for the square lattice, the numerical model for the hexagonal lattice also shows an asymmetry in buckling across the row of inclusions. The top half shows a clear pattern transformation, while the bottom half has only a small amount of shearing. Most of the deformation in the bottom half is compression of the voids. This result matches the experimental results closely. The pattern change in only the top half of the lattice is a result of an asymmetry in the imperfections placed in the lattice to induce the buckling mode. A slightly different pattern of imperfections in the bottom half of the lattice creates enough of a difference between the two halves to allow for the pattern transformation to be preferentially triggered on only one side. In both the experimental and numerical results an asymmetry across the row of inclusions can lead to the pattern transformation being preferentially triggered on the side that requires the lowest critical stress. Once the pattern is triggered on one side the inclusions act as a barrier to prevent the pattern from being initiated on the other side.

4.2.3 Reducing the Stiffness of the Inclusions

In all of the previous cases the stiffness of the inclusions was kept approximately the same. At that fairly high stiffness, pattern change in the region with inclusions was almost completely suppressed, and was also suppressed to a lesser degree in the voids surrounding the inclusions. By decreasing the stiffness of the inclusions, the buckling of the ligaments around the holes with inclusions can occur at a lower critical stress.

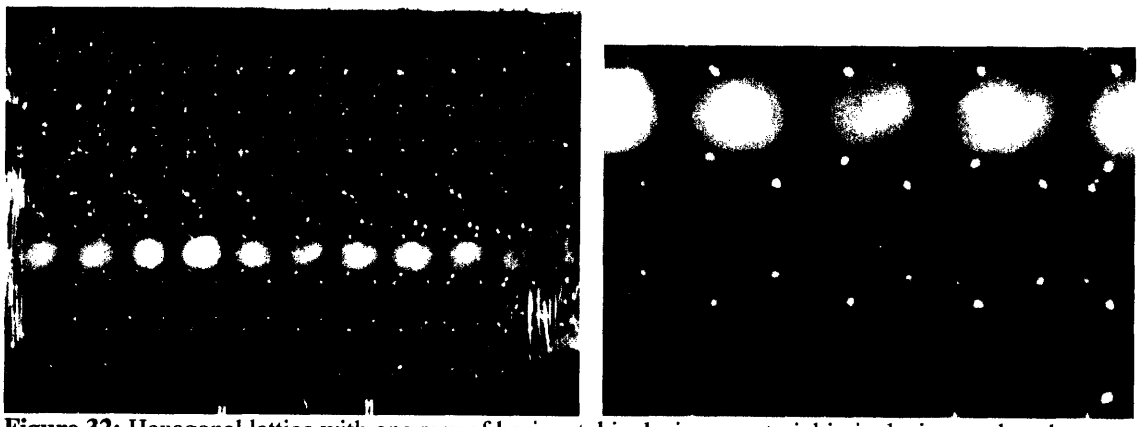

Figure 32: Hexagonal lattice with one row of horizontal inclusions, material in inclusions reduce by one half from previous cases

Figure 32 demonstrates that while the pattern change below the inclusions is much less accentuated than above it, there is some shearing of the voids. This transformation below the inclusions was not evident in the case with the higher stiffness inclusions. The row of inclusions no longer acts as a barrier to pattern change because these holes now also show some shearing. The decreased stiffness allows the shear instability to be triggered even with inclusions next to the ligaments. The inclusions still act to suppress the pattern change to some extent, and the shearing of the voids is much more pronounced above the row of inclusions.

Further decreasing the stiffness of the inclusions results in even less suppression of the pattern transformation.

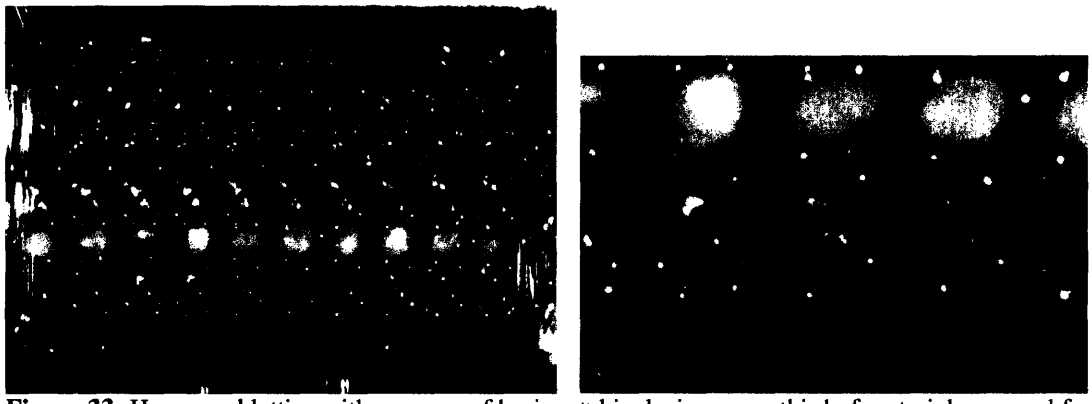

Figure 33: Hexagonal lattice with one row of horizontal inclusions, one third of material removed from previous case

In Figure 33 further accentuation of the sheared pattern can be seen in both the holes with inclusions and the empty row below them. The amount of shearing that the rows below the inclusions experience is dictated by the stiffness of the inclusions. Different inclusion stiffnesses result in different degrees of pattern change. The row of inclusions acts to control the amount of shearing that occurs below it.

5. Conclusion

The mechanics of the deformation of elastomeric sheets with both square and hexagonal lattices of voids cut into them were tested. The pattern changes of these lattices was investigated both with the plain structure, and then with inclusions introduced in different patterns and stiffnesses. Finite element analysis was also used to study the deformation of the lattices. With both structures unique pattern transformations were observed. These transformations were the result of local instabilities in the structure. A buckling instability in the square lattice and a shear instability in the hexagonal lattice resulted in different pattern changes for the two cases. Adding inclusions into the voids resulted in even more unique patterns, mimicking the higher buckling modes of the lattice with no inclusions.

For some of the patterns of inclusions, the results could be predicted accurately through finite element analysis, and also by looking at the pattern of the buckling mode that was being mimicked. The higher buckling could be accurately reproduced by suppressing the first mode. This result shows that the pattern change produced can be controlled. It has been show previously that the spacing between voids as well as the size of the voids affects the load at which the pattern change occurs, and can be predicted. The type of lattice used also results in different and predictable pattern transformations. The pattern change initiated in a structure under compression can therefore be controlled on many levels. The results indicate that a highly detailed pattern change can be dictated by controlling the parameters of the lattice and the inclusions.

Having the inclusions perpendicular to the direction of compression did not demonstrate the results predicted by finite element analysis, but still provide interesting insight into the controllability of pattern change. At high stiffnesses the inclusions acted

as a barrier to pattern change below the row that they occupied. This barrier could be used to localize a pattern change in one area of the lattice, or to create a sheet where the pattern is suppressed below a certain point. This barrier could possibly also be used to create pockets in a large lattice where the pattern is present. Decreasing the stiffness of the inclusions allows the pattern change to occur below the lattice, but to a lesser degree. Because lower stiffnesses allow more accentuation of the pattern change, the extent to which the pattern is changed can be tuned by changing the stiffness of the inclusions. Different levels of accentuation can therefore be seen in the same lattice.

All of the results seen indicate the ability to create a lattice that is tuned to have pattern transformations that can be predicted by controlling the parameters of both the lattice and the inclusions. With just two different lattices and a few patterns of inclusions a wide array of pattern changes is seen. Further investigation into different arrays of inclusions could lead to many more instances of new, predictable patterns.

The results of this investigation are on a millimeter-length scale, but the effects should persist at the micro- and nano-scale. At these smaller scales, the transformations could lead to applications in photonic and phononic crystals. The structures could have the ability to manipulate light and sound. With the pattern being controlled by the parameters of the lattice, the behavior of the light and sound could also be controlled. The many different manners in which the pattern change can be controlled indicate that a highly detailed level of control of the light or sound could also be possible, and specific functions may be achieved.

References

Bertoldi, K., Boyce, M.C., Deschanel, S., Prange, S.M., Mullin, T, 2007. "Mechanics of Deformation-Triggered Pattern Transformations in Periodic Structures," submitted for consideration for publication to Journal of the Mechanics and Physics of Solids

Gibson, L.J., Ashby, M.F., 1997. Cellular Solids: Structures and Properties. Cambridge University Press.

Mullin, T., Deschanel, S., Bertoldi, K. Boyce M.C., 2007. "Pattern Transformation Triggered by Deformation", accepted for publication in Physical Review Letters.